Extreme Wildfire Environments and Their Impacts Occurring with Offshore-Directed Winds across the Pacific Coast States

JONATHAN M. GARNER[a] AND CARLY E. KOVACIK[b]

[a] *NOAA/National Weather Service, Eureka, California*
[b] *NOAA/National Weather Service, Seattle, Washington*

(Manuscript received 30 March 2022, in final form 30 November 2022)

ABSTRACT: Wildfires that posed an immediate threat to life and property during the period 1933–2021 were examined across the Pacific Coast states of California, Oregon, and Washington. Such fires were identified in local, state, and federal data archives and other sources that yielded 150 events for analysis. A subset of those fires was sorted into one of two synoptic-scale patterns associated with an autumn-season offshore-directed low-level flow regime and a summer-season non-offshore-directed low-level flow regime. Proximity analysis soundings near the offshore wind-driven wildfires frequently displayed ingredients that supported gap and mountain-wave development, which were responsible for generating fast-moving wildfires, long-distance spotting, and firebrand showers that resulted in loss of life and property. Paradoxically, the most extreme combinations of strong winds and low relative humidity were observed near high-population centers in Southern California, yet the most destructive and deadly fires were in less-populated regions of northern California and western Oregon. Additional analysis of 40 Fire Behavior Fuel Models data, housing development in the wildland–urban interface, and U.S. census demographic information revealed that the northern California and western Oregon wildfires were associated with more devastating outcomes because 1) a higher ratio of communities were intermixed with flammable fuels, 2) fire ignitions of an electrical origin occurred in wind-prone corridors that were upstream from communities, and 3) communities in northern California and western Oregon were composed of a greater percentage of socially vulnerable people such as the elderly who were less capable of perceiving and evading intense rapidly evolving wildfires.

KEYWORDS: Forecasting; Forest fires; Societal impacts

1. Introduction

The threat of violent wildfires resulting in mass casualties and the destruction of entire communities has seemingly become a way of life across the Pacific Coast states of California, Oregon, and Washington (Westerling 2016; Goss et al. 2020). The most extreme events have been uncontrollable from a firefighting perspective and have often evolved into life-saving evacuations. The October 1991 East Bay Hills Fire, which killed 25 people in the communities of Oakland and Berkley, was a prelude to the modern fire regime. Strong offshore winds yielded extreme fire behavior that led to a situation in which evacuation was nearly impossible because of fast rates of spread occurring in the midst of complex terrain and narrow restricted road systems (FEMA 1995). The East Bay Hills Fire of 1991 was followed by devastating wildfire outbreaks in San Diego County during October 2003 that killed 24 people and then the 2007 Harris Fire that killed another 8 people. More recently, the San Francisco North Bay counties of Sonoma, Napa, and Mendocino experienced an outbreak of wildfires during early October 2017 that killed 44 civilians (Nauslar et al. 2018). One year later, the 8 November 2018 Camp Fire essentially destroyed the city of Paradise, California, and produced 86 fatalities (Mass and Ovens 2021). Additional wind-driven wildfires were observed farther north across the west slopes of the Cascade Range in Oregon during September 2020, which led to the destruction of 4500 structures and the deaths of 9 people (Mass et al. 2021). Roughly 68% of the fatalities attributed to the North Bay and Camp Fires were in the 65–89-yr age range, with many elderly succumbing to those fires because of limitations in mobility and perception. Documented elderly evacuations were hindered by disabilities, an inability to operate a vehicle, and illness that left them bedridden. Other victims had dementia or were socially isolated from their communities. Those circumstances led to deaths that often occurred within or near a place of residence (Garner et al. 2020).

These devastating events are primarily a late-summer–early-winter phenomenon and develop when strong offshore winds are generated by 1) mountain-wave windstorms occurring in the lee of terrain barriers, or 2) within terrain gaps and their exit regions. Both wind regimes are spatially correlated with elongated topographic barriers that are collocated with strong cross-terrain-oriented pressure gradients. Mountain-wave and gap wind environments can occur simultaneously and in close proximity to each other (Mass and Albright 1985; Colman and Dierking 1992; Blier 1998; Colle and Mass 1998)—thus their environments often appear similar. Ingredients supporting their development include 1) strong cross-barrier flow, 2) a ridgetop inversion (Brinkmann 1974; Klemp and Lilly 1975), and 3) a critical

Supplemental information related to this paper is available at the Journals Online website: https://doi.org/10.1175/WCAS-D-22-0043.s1.

Corresponding author: Jonathan M. Garner, jonathan.garner@noaa.gov

DOI: 10.1175/WCAS-D-22-0043.1

level generally located in the midlevels of the troposphere (Klemp and Lilly 1978; Clark and Peltier 1984; Durran and Klemp 1987; Colman and Dierking 1992). The change in stability associated with the ridgetop inversion and a critical level in which wind speed decreases to zero in the midlevels, or when the wind reverses in direction (Colle and Mass 1998), have been shown in numerical simulations to aid in wave amplification due to downward reflection of upward propagating wave energy. Colman and Dierking (1992) presented conditions supporting mountain-wave development in the vicinity of Juneau, Alaska, that featured cross-barrier flow of 15–20 m s^{-1}, an inversion between 1.5 and 2.0 km above mean sea level (MSL), and a critical level located between 3.0 and 5.5 km MSL. In addition, composite soundings generated by Brinkmann (1974) for mountain waves occurring near Boulder, Colorado, revealed ridgetop inversion heights generally located between 3.0 and 5.0 km MSL, while a mountain-wave windstorm in the lee of the Wasatch Range in Utah featured cross-barrier flow of ~30 m s^{-1} (Lawson and Horel 2015) positioned 500 m above ridgetop level. Mountain-wave scenarios have also been documented outside of the United States, such as Greece during 23 July 2018, in which downslope winds drove a destructive deadly firestorm through the city of Attica (Lagouvardos et al. 2019).

The synoptic-scale evolution leading to strong offshore wind events across the Pacific Coast states has been well-documented in the literature. For example, National Weather Service training material from 1999 identified a midlevel ridge over the northeast Pacific and trough over the western United States as a favorable synoptic pattern for offshore winds in the vicinity of Medford, Oregon. In addition, an embedded disturbance moving southeast between the ridge and trough combined with cold advection associated with surface high pressure were favorable for strong Santa Ana winds in Southern California (NWS 1999). Those features have been highlighted in other offshore wind studies, such as Huang et al. (2009), Mass and Ovens (2019), McClung and Mass (2020), Mass and Ovens (2021), and Mass et al. (2021). A large temperature gradient between cold inland areas and the warmer Pacific Ocean was also shown to be a primary driver for strong offshore winds in a study by Hughes and Hall (2010). Similarly, Abatzoglou et al. (2013) concluded that low-level cold air combined with a tight northeast surface pressure gradient provided a robust means of diagnosing Santa Ana wind development in Southern California. Further evidence exists of strong cross-barrier flow being driven by the juxtaposition of cold dense air against a terrain barrier and less dense air on the lee side, such as Doran and Zhong (2000), who showed that gap winds occurring in the southeast corner of the Mexico City Basin were most intense when temperature differences across a terrain barrier were strongest. Similarly, Sharp and Mass (2004) demonstrated that easterly gap winds occurring through the Columbia River Gorge were most likely when a negative temperature anomaly at 850 hPa was located over Montana and eastern Washington, and Neiman et al. (2019) showed those gap wind events were stronger and longer-lived when forced by cold-interior anticyclones, while weaker events occurred when the terrain-oriented pressure gradient was forced by an offshore cyclone.

The identification of gap and mountain-wave wind regimes is operationally important because they support extreme rates of fire-front spread, tilted fire plumes, preheating of downstream fuels, long-range spotting, and firebrand showers. The process of spotting involves a firebrand launched vertically by a fire plume. The firebrand experiences a combustion lifetime[1] as it is transported horizontally by the wind and is then deposited upon the surface due to factors such as gravity, drag, and buoyancy. The initiation of new fire occurs if weather and fuel conditions combined with a sufficient firebrand combustion life span are present (Martin and Hillen 2016). The area impacted by combustible firebrands is a function of mass and wind, with stronger wind speeds yielding a greater number of firebrands, as well as more massive firebrands such as those emanating from shrubs and trees (Bahrani 2020). It has also been shown experimentally that the accumulation of large numbers of firebrand shower particles within human built structures increases the potential for ignition (Manzello et al. 2020). This is problematic for northern California communities in regions such as the foothills of the Sierra Nevada, which have experienced growth almost exclusively within the urban–wildland interface (Hammer et al. 2007). Furthermore, long-range spotting and firebrand showers can overwhelm wildland fire suppression efforts, and also contribute toward wildland–urban interface (WUI) conflagrations as firebrands encounter flammable materials within roofs and other housing materials, which can then yield structure-to-structure fire spread (Koo et al. 2010; Tohidi and Kaye 2017; Keeley and Syphard 2019). That kind of extreme fire behavior was observed during the 1991 East Bay Hills Fire, with spot fires occurring 0.4 km ahead of the flame front (FEMA 1995). Similarly, gusts exceeding 22 m s^{-1} produced spot fires during the 2018 Camp Fire that were responsible for preignition of shrubs, bushes, and trees located several kilometers from the flame front and deep within Paradise. Extreme gusts also contributed to burnovers during the Camp Fire that led to firefighter and civilian entrapments that significantly impacted evacuation from town and, in some cases, led to injuries and fatalities (Maranghides et al. 2021).

This paper compares and contrasts extreme fire weather environments typical of Santa Ana–type events in Southern California with offshore-directed wind-driven wildfires in northern California and the Pacific Northwest. That is accomplished by synthesizing a West Coast centric multidecade multifire dataset with previous literature focused on extreme Pacific Coast wildfires. Such an analysis has not been identified in preexisting peer-reviewed literature, and thus could be a beneficial resource for operational weather forecasters, wildland firefighters, hazard mitigation agencies, and government decision makers tasked with warning and protecting the public against potentially deadly wildfires. Meteorological similarities and differences for both the Southern California and northern California/Pacific Northwest regions are addressed through an analysis of the thermodynamic and kinematic environments

[1] Combustion lifetime is the period of time in which an ember is flammable.

TABLE 1. Data types utilized for study, their period of availability, and a description of those data and where they can be located on the internet.

Data type	Time span	Description
HYSPLIT	2000–present	Backward model parcel trajectories from the location of each fire (https://www.ready.noaa.gov/HYSPLIT.php)
Storm Events database	1950–present	A record of impactful storms and significant weather phenomena (https://www.ncdc.noaa.gov/stormevents/)
Historical surface obs	2000–present	Archived ASOS, AWOS, and mesonet obs used to analyze surface temperature, relative humidity, wind speed and direction, and MSLP (https://www.wrh.noaa.gov/map/)
North American Regional Reanalysis	1979–present (minus 1-month lag from the present)	Synoptic analysis of upper-air heights and surface MSLP (https://psl.noaa.gov/cgi-bin/data/narr/plothour.pl)
North American Ensemble Forecast System	2017–present	Analysis of standardized temperature anomalies (https://satable.ncep.noaa.gov/archive)
RUC and RAP 0-h analysis soundings	RUC: 2011; RAP 2012–21	Proximity soundings to wildfires used to assess mountain-wave ingredients (https://mtarchive.geol.iastate.edu/)
xmACIS2	1992–2021	Daily temperature and precipitation data over a multiyear period near the site of each wildfire (https://xmacis.rcc-acis.org/)
Drought Monitor	2000–present	Multiyear drought classification (https://droughtmonitor.unl.edu/maps/maparchive.aspx)
40 Fire Behavior Fuel Models	None	Gridded fuel classification at the site of each fire (https://landfire.gov/fbfm40.php)
U.S. Census QuickFacts	2011–21	Demographic information for all counties impacted by wildfire in the current study (https://www.census.gov/quickfacts/fact/table/US/PST045221)
Wildland–urban interface	1990–2010	County-based classification of area, population, and housing intermixed or interfaced with fuels (https://www.fs.usda.gov/rds/archive/Catalog/RDS-2015-0012-2)

that result from synoptic and mesoscale systems interacting with the terrain of the West Coast. A more complete picture of extreme wildfire outcomes is then accomplished by supplementing the environmental analysis with data related to regional fuels, human development in the wildlands, and county-based plus fire-specific demographics. Methods for this study are presented in section 2. Section 3 further expands on the background and study area for this paper, and results are given in section 4. Those results are followed by conclusions and a discussion in section 5.

2. Methods

Wildfires occurring across the states of California, Oregon, and Washington during the period 1933–2021 were evaluated for extreme behavior that posed an immediate threat to life and property. Such behavior included any wildfire that approached or entered a populated area leading to evacuation, destruction of human-built structures, injuries, or loss of life. Those types of fires, as well as their associated impacts, were identified in local, state, and federal fire agency documents as well as National Centers for Environmental Information (NCEI) Storm Events Data. Secondary sources of information included media news reports, published research, and other summaries such as those found through Wikipedia. A list of wildfires compiled from the above sources was augmented with fatality information, including the circumstances associated with each wildfire death, age-related fatality information, and the location and time of extreme fire behavior and impacts, as well as fire-ignition cause and location. Fires were also divided into a northern and southern analysis area based on whether they occurred north or south of 37.45°N latitude, an east–west line that goes through the southern tip of San Francisco Bay.[2] U.S. census data were then used to determine the median age of each county impacted by wildfires, as well as the percentage of county population aged 65 or greater, and growth statistics such as population per square mile and the percent change in population over a 100-yr period. Impacted counties were also compared with a geospatial dataset of the wildland–urban interface created and maintained by the U.S. Forest Service (Radeloff et al. 2017), which was used to analyze at a countywide scale the percent of housing and population intermixed or interfaced with fuels.

The HYSPLIT model (Table 1) was used to produce 48-h backward parcel trajectories, and it was found that offshore-directed[3] versus non-offshore-directed wind-driven wildfires could be grouped into two different trajectory categories. Trajectories associated with offshore-directed winds took anticyclonic paths from western portions of Canada and the CONUS toward the Pacific Ocean. On the other hand, trajectories occurring with

[2] Hereinafter all references to northern/southern area, northern/southern analysis area, or northern/southern events are referring to wildfires occurring either north or south of 37.45°N latitude.

[3] Hereinafter, mention of offshore wind is defined as an offshore-directed wind. Similarly, an offshore event is in reference to a wildfire associated with offshore-directed surface winds.

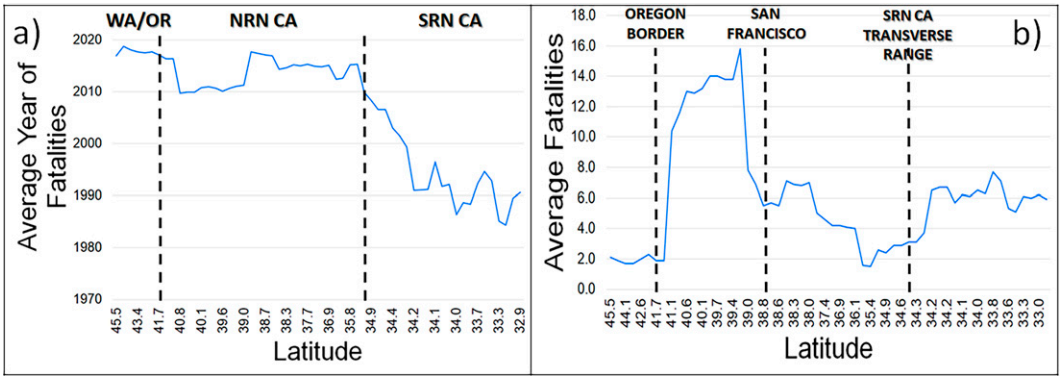

FIG. 1. Analysis during the period 1933–2021 of (a) the average year in which fatal wildfires occurred with respect to latitude and (b) the average number of wildfire fatalities with respect to latitude. Fatality data were paired with an associated latitude, which was then used to compute a north-to-south 10-point latitudinal moving average of the year in which fatalities occurred, as well as the fatalities produced by each fire. The geographical locations of Washington and Oregon (WA/OR), northern California (NRN CA), and Southern California (SRN CA) are annotated in (a), and the Oregon border, San Francisco, and the Southern California (SRN CA) Transverse Range are annotated in (b).

non-offshore-directed wind regimes were either parallel to the coast or moved from the Pacific Ocean onshore across the West Coast of the United States. Offshore-directed wind classifications were further augmented by ensuring that observed surface wind directions possessed an easterly component.[4] The 1° Global Data Analysis System[5] (GDAS) from 2006 to the present was the first data source utilized for backward trajectories. However, the Global Forecast System (GFS)[6] was available from 2019 to the present, the North American Mesoscale Forecast System (NAM)[7] was available from 2007 to the present, and a global reanalysis was available from 1948 to the present. Those alternative model data sources were considered if the GDAS was unavailable or produced backward trajectory paths that failed to emanate away from the source point. Otherwise, the length of each trajectory was recorded, as well as the height in which the parcel originated from, and the change in relative humidity occurring from the start and finish of the parcel path.

Surface variables representing the wildfire environment were evaluated for events occurring during 2000–21 by matching the time and location of extreme fire impacts with the nearest surface observing station in a valley as well as on a ridge[8]—a method that is believed to have represented the range of environmental conditions experienced during the most extreme stage of a fire.[9] Any ASOS, AWOS,[10] or mesonet surface observation was considered for inclusion in the analysis after passing a subjective check for consistency with surrounding observations and the general synoptic-scale thermodynamic and kinematic regime. Variables recorded from each surface observation included sustained wind speed, maximum wind gust, temperature, relative humidity, and mean sea level pressure (MSLP). The Fosberg fire weather index (FFWI; Fosberg 1978) was also derived for each observation. In addition, surface observations spanning terrain barriers were used to compute temperature and MSLP gradients that might contribute to thermally driven winds, including gap and cross-barrier flows. Terrain classifications were also assigned by plotting the location of each wildfire in Google Earth. The topographic features collocated with each fire plotted in Google Earth were compared with archived mesonet wind directions, which aided in the designation of one of four terrain types: 1) gap wind regime characterized by archived winds directed through a gap in an elongated topographic feature; 2) leeside ridge in which winds were perpendicular to an elongated topographic feature and wildfire occurred downwind near the base of the topography; 3) crest of a ridge, which was primarily identified when wildfire occurred along the crest of an elongated topographic feature; and 4) valley parallel flow regime characterized by surface winds and fire spreading parallel to and between two elongated topographic features.

The synoptic-scale regime leading to both offshore- and non-offshore-directed low-level winds was assessed through

[4] The average wind direction for offshore-directed wind-driven wildfires was 77°.

[5] More information on the GDAS is available online (https://www.ncei.noaa.gov/products/weather-climate-models/global-data-assimilation).

[6] More information on the GFS is available online (https://www.emc.ncep.noaa.gov/emc/pages/numerical_forecast_systems/gfs/documentation_spectralgfs.php).

[7] More information on the NAM is available online (https://www.emc.ncep.noaa.gov/emc/pages/numerical_forecast_systems/nam/NAM_2017.pdf).

[8] The mean distance between observation sites and wildfires was 18.4 km, with a standard deviation of 13.4 km.

[9] The environmental analysis presented in section 4 is limited to the period 2000–21 because that is the period in which the record of surface observations is complete. Otherwise, societal impacts, such as fatalities, are derived from the full 1933–2021 dataset.

[10] ASOS stands for automated surface observing station, and AWOS stands for automated weather observing system.

TABLE 2. Minimum acres burned, maximum acres burned, average acres burned, average structures destroyed, and average fatalities for northern offshore-directed wind-driven wildfires (offshore north), southern offshore-directed wind-driven wildfires (offshore south), northern non-offshore-directed wildfires (non-offshore north), and southern non-offshore-directed wildfires (non-offshore south) valid from 2000 to 2021. The "northern" area comprises northern California, western Oregon, and Washington, and the "southern" area is composed of the southern portion of California located south of San Francisco Bay to the Mexico border.

	Min acres burned	Max acres burned	Avg acres burned	Avg structures destroyed	Avg fatalities
Offshore north	80	318 930	72 644	1465	6.2
Offshore south	154	281 893	43 966	306	1.2
Non-offshore north	10	1 032 648	106 838	212	0.7
Non-offshore south	278	380 002	45 151	118	0.5

multifire composite charts created with North American Regional Reanalysis (Mesinger et al. 2006) surface and upper-air data. In addition, a 0-h Rapid Update Cycle (RUC; Benjamin et al. 2004) or Rapid Refresh (RAP; Benjamin et al. 2016) forecast model buffer sounding located nearest to each wildfire was archived and analyzed for events occurring from 2011 to 2021. Information from those soundings was used to deduce the presence of ingredients[11] supportive of mountain-wave development. Cursory meteorological analyses were also performed on NEXRAD data obtained from NCEI to assess the occurrence of fire mesocyclones (Lareau et al. 2018, 2022). These analyses yielded limited statistical results due to poor radar viewing angles and are not further discussed in this paper. Otherwise, information related to fuels and climate was evaluated. However, archived fuel data were not readily available for analysis during the data collection phase of this project. Thus, vegetation dryness was inferred through various data sources. First, the background temperature and precipitation near the site of each fire over a 30-yr period spanning 1992–2021[12] was examined using xmACIS2. Seasonal temperature and precipitation anomalies were then examined for the region in which a fire occurred using the same 30-yr average,[13] and standardized temperatures anomalies in the 1000–700-hPa layer were assessed using the North American Ensemble Forecast System. Otherwise, a slightly more direct qualitative assessment of vegetation dryness was deduced using drought intensity via archived U.S. Drought Monitor information.

3. Background and study area

The distribution of extreme wildfires and their impacts displayed substantial variability in both space and time across the Pacific Coast states. For instance, a moving average of fatalities with respect to latitude shows that deadly Southern California events were clustered around the year 1990 (Fig. 1a). The average year of deadly wildfires then shifts north into northern California, western Oregon, and Washington during the period 2010–20. In addition, fires yielding the most fatalities and structures destroyed occurred within a relatively narrow latitudinal range located immediately north of San Francisco Bay into west-central Oregon (see Fig. 1b and Table 2)—and that remained true even with the outlier 2018 Camp Fire[14] removed from the analysis. Furthermore, the most extreme fires in terms of death and destruction were not the fires that burned the highest average number of acres (1 acre ≈ 0.4 ha). Instead, high-acreage events occurred across remote regions over a multiweek–multimonth time period during the warmest times of the year when strong synoptic-scale wind regimes were less probable. Examples of those types of large acreage fires yielding zero civilian fatalities include the 459 123 acre 2018 Mendocino Complex, the 963 309 acre 2021 Dixie Fire, and the 2020 August Complex that burned over one million acres—all of which occurred in northern California.

Wildfires of the Pacific Coast states[15] occurred across a vast and diverse geographic setting. Mountain chains were generally long in the north–south direction and narrow in the east–west direction—such as the 1100-km-long Cascade Range and 640-km-long Sierra Nevada, both of which were ~130 km wide (Fig. 2). North of the Cascade Range, the 2000-m-high Okanogan Highlands and their north–south river valleys were located in northeastern Washington, the Columbia Basin comprised a large portion of southeastern Washington, and the Puget Sound lowlands encompassed the area immediately west of the Washington Cascades. Farther south, a coastal range of north–south trending ridges and mountains extended from San Francisco Bay northward across northwestern California into southwestern Oregon. East of that area, the southern terminus of the Cascade Range transitioned to the Sierra Nevada, which extended southeastward from northeastern California to Lake Tahoe and then south-southeast to the northern periphery of the Mojave Desert in Southern California. Elsewhere, the Great Basin extended southeast from southeastern Oregon along the east side of the Sierra Nevada and then eastward across much of Nevada. The southern Great Basin then transitioned to the Mojave Desert, and farther west, the Mojave Desert gave way to the Transverse Range, which extended west from

[11] Refer to section 1 for a description of mountain-wave ingredients.

[12] Yearly anomalies were only included for study if missing data were less than 30 days.

[13] Those data are available online (https://psl.noaa.gov/data/usclimdivs).

[14] The 2018 Camp Fire killed 86 people. The next highest fatal event in the dataset was the 2017 North Bay wildfire outbreak, which killed 40 people.

[15] See Tables S1–S4 in the online supplemental material for a list of wildfires included in the environmental analysis of this paper.

FIG. 2. Annotated physiographic provinces and coastal cities of the Pacific Coast states. The elevation scale is kft (1 kft = 304.8 m).

southwestern San Bernardino County, California, across central Los Angeles County into Ventura and Santa Barbara Counties. To the south of the eastern Transverse Range was the Peninsular Range, which was located immediately east of San Diego, California, and north of the western Transverse Range was the Coast Range, which extended northward along the California coast to the San Francisco Bay Area. The large north–south-oriented Central Valley was positioned between the California Coast Range and the Sierra Nevada.

Plotted wildfires occurring north of the latitude 37.45°N were generally clustered within the Coast Range immediately north of San Francisco, the western foothills of the northern Sierra Nevada, the western foothills of the Cascade Range in Oregon and Washington, and the southern periphery of the Okanogan Highlands in northcentral and northeast Washington (Figs. 3a,c). Figure 3b shows that all southern offshore-directed wind events occurred within the Transverse Range of Southern California southward through the Peninsular Range. In addition, a thorough search of fire records yielded no extreme offshore-directed wind-driven events between the Transverse Range and San Francisco Bay, as well as the west side of the southern Sierra Nevada. Otherwise, non-offshore-directed wind events were clustered within the Coast Range south of the San Francisco Bay Area, the west side of the southern Sierra Nevada, the Transverse Range, and the Peninsular Range (Fig. 3d).

All wildfires examined were sorted into four topographic categories identified by plotting the latitude and longitude point of each fire within Google Earth. Those categories included terrain gaps, the lee side of a ridge-oriented perpendicular to low-level cross-barrier flow, the crest of a ridge, or a position within a valley in which the low-level flow was parallel to the long-axis of the valley. Roughly 55% of northern offshore-directed, 75% of southern offshore-directed, and 60%–70% of non-offshore-directed wind events were located within a gap or its exit region (Fig. 4). Approximately 20%–40% of northern and southern offshore-directed wind events were also found to occur in the lee of a ridge, while less than 5% of non-offshore events were in the lee of a

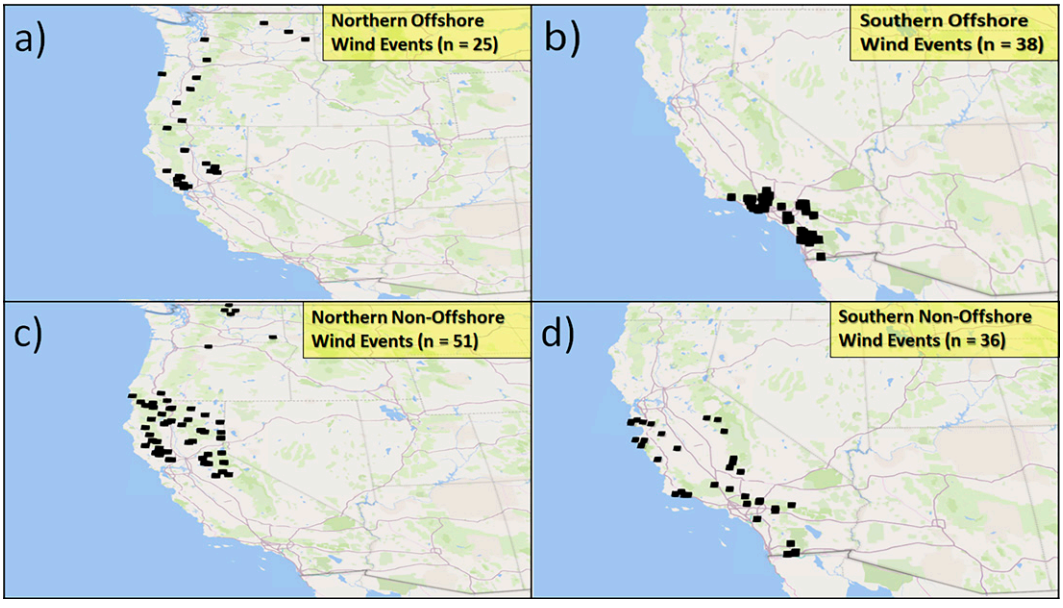

FIG. 3. Wildfires (black squares) included in the environmental analysis period 2000–21 for offshore-directed winds occurring (a) north of 37.45°N latitude and (b) south of 37.45°N latitude and for non-offshore-directed wind-driven wildfires occurring (c) north of 37.45°N latitude and (d) south of 37.45°N latitude.

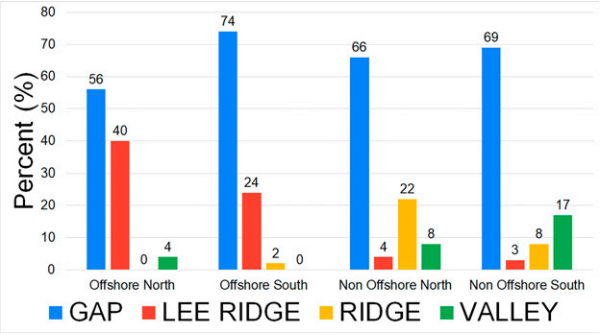

FIG. 4. Percent distribution of terrain settings associated with wildfires occurring during the period 1933–2021 for offshore-directed winds occurring (a) north of 37.45°N latitude (Offshore North) and (b) south of 37.45°N latitude (Offshore South) and for non-offshore-directed wind-driven wildfires occurring (c) north of 37.45°N latitude (Non Offshore North) and (d) south of 37.45°N latitude (Non Offshore South).

ridge. These topographic settings were associated with specific geographic regions across the Pacific Coast states. For example, 100% of the North Bay Hills composed of Mendocino, Lake, Sonoma, and Napa Counties featured offshore-directed wildfires that occurred in the lee side of a ridge. On the other hand, 79% of the wildfires occurring from the Okanogan Plateau south across the western foothills of the Oregon Cascades and farther south across the west side of the northern Sierra Nevada occurred within gap terrain features. Elsewhere, the Transverse and Peninsular Ranges of Southern California, although strongly favoring offshore-directed gap wind events (74%), were also interspersed with leeside ridge events (23%).

4. Results

a. The synoptic setting

Consistent with past literature (NWS 1999; Huang et al. 2009; Mass and Ovens 2019; McClung and Mass 2020; Mass and Ovens 2021; Mass et al. 2021), analyzed wildfires occurring with offshore-directed winds were associated with a composite 500-hPa height chart featuring an anomalous northeast Pacific Ocean ridge and western/central U.S. trough (Fig. 5). The composite upper-level ridge for both northern and southern offshore-directed wind events featured a positive height anomaly of 180 m located offshore from Washington, and a negative height anomaly of −90 (northern) and −60 (southern) m centered over southern Manitoba, Canada, and the north-central CONUS. Examination of individual cases also revealed a shortwave trough moving southeast between the synoptic-scale ridge and trough (see Fig. 6a for an example). Those shortwaves are smoothed out in the composites presented in Fig. 5, but 79% of northern and 73% of southern offshore-directed wind-driven wildfires occurred in the wake of a passing 500-hPa shortwave trough, and 17% and 22%, respectively, occurred directly beneath a shortwave trough. The passage of the midlevel wave is generally collocated with cold air in the low-levels spreading south along the east side of the Cascade and Sierra Nevada[16] (Fig. 6b). That cold air mass is evident in composite temperature anomalies in the 1000–700-hPa layer, which showed a −6°C minimum centered approximately over eastern Montana and Wyoming (Fig. 7). Furthermore, the western periphery of anomalously cold air was positioned immediately adjacent to the east side of the Sierra Nevada and Cascade Range, while warm anomalies were positioned on the west side of those mountain chains over the Pacific Coast. Such a configuration of air masses blocked by terrain barriers favors wind accelerations directed from the cold air mass toward the warmer wherever weaknesses in the topography are encountered.

An ensemble of model backward parcel trajectory analyses over a 48-h time period starting from the location of each analyzed fire are presented in Figs. 8 and 9. Parcels participating in both northern and southern offshore-directed wind events generally originated from the crest of an upper-level ridge positioned over the northeastern Pacific Ocean or western Canada. The mean height of parcel initiation ranged between 3.4 and 3.9 km above ground level (AGL), and the average length of the parcel trajectories was 2232–2331 km (Table 3). For northern offshore-directed wind events, parcels took an anticyclonic path as they descended toward the fire location, eventually approaching the surface from the east for events in Washington and Oregon, or from the north-northeast in northern California. The northern California events in particular appeared to follow a path that remained north of the Sierra Nevada, and south of the Cascade Range. Parcels that descended in between both mountain chains continued a southern course through the northern Central Valley of California before turning westward and exiting across the Coast Range located immediately north of the Golden Gate terrain gap. Southern offshore-directed trajectories took an anticyclonic path around the east side of the Sierra Nevada, assumingly due to air flowing toward the mountains in a stably stratified atmosphere (Chen and Smith 1987). Parcels then descended across the Mojave Desert south of the Sierras before reaching the surface in the Southern California Transverse and Peninsular Ranges. For the cases examined, the blocking effect of the Sierra Nevada, and subsequent lack of strong cross-barrier flow, appeared to preclude offshore-directed wind-driven wildfires across the Coast Range south of San Francisco Bay, and also precluded events across the western foothills of the central and southern Sierra Nevada. Otherwise, for non-offshore fire regimes, parcel trajectories appeared to be dominated by the presence of surface high pressure located over the northeast Pacific Ocean, and low pressure over the Intermountain West—which are features typical of the summer months (Taylor et al. 2008). That surface pressure configuration resulted in parcel trajectories that were fundamentally different from the offshore-directed trajectories. For example, non-offshore trajectories were generally parallel to the Pacific Coast or took a path that turned inland during final approach to a fire (Fig. 9). In addition, these non-offshore-directed parcels originated much closer to fires

[16] The midlevel shortwave trough could also serve as a critical level if wind speed within the trough decreases to near zero.

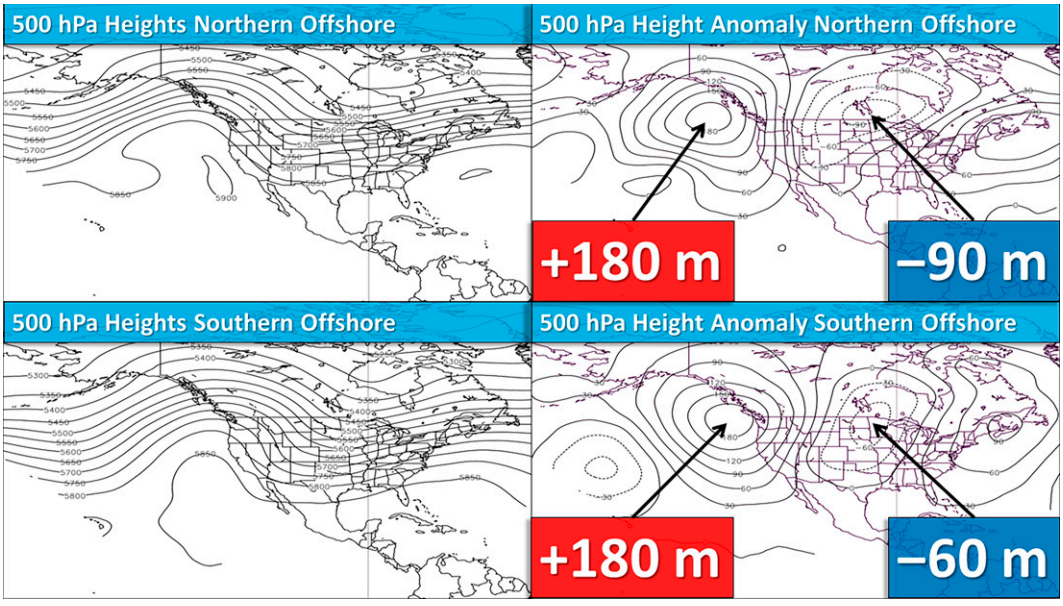

FIG. 5. Mean composite 500-hPa (left) heights (m) and (right) height anomalies (m) for (top) northern and (bottom) southern offshore-directed wind-driven wildfires examined for the period 2000–21. Composite charts were created using the North American Regional Reanalysis. Positive (+) and negative (−) height anomalies are annotated in the right panels. Images were provided by the NOAA/ESRL/Physical Sciences Laboratory (https://psl.noaa.gov/cgi-bin/data/narr/plotday.pl).

(mean distance of 577 km), and their average initial height AGL was much lower (~0.6 km). In addition, stronger drying occurred during the life span of parcel trajectories associated with offshore-directed wind events [mean change in relative humidity (RH) of −38%] in comparison with the non-offshore-directed events (mean change in RH of −25%).

b. *The mesoscale environment*

Hughes and Hall (2010) as well as Abatzoglou et al. (2013) describe intense mesoscale pressure gradients that are generated across the complex terrain of the Pacific Coast states when cold dense air becomes situated over the Intermountain West, Great Basin, and Mojave Desert, and is blocked from descending toward warmer and less dense air positioned near the Pacific Coast. Those processes were qualitatively observed in the current study for most offshore-directed wind events and were also documented in a quantitative sense. For example, the cross-barrier difference in 850-hPa potential temperature derived from regional raob data averaged 5.0°C for the northern analysis area, and 7.4°C for southern events. Southern offshore-directed wind events were also associated with a colder average inland surface temperature (13.0°C) and stronger average cross-terrain surface temperature gradient (0.14°C km^{-1}) relative to northern events (16.3° and 0.06°C km^{-1}, respectively). The colder surface conditions and tighter temperature gradients accompanying southern offshore-directed wildfires were believed to result from a greater percentage of events occurring deeper into the late-autumn and early-winter seasons (37% from November through January) in comparison with northern events (4%). In addition, cold air over the Mojave Desert was situated closer to warmer lee-side air positioned west and south of the Peninsular and Transverse Ranges, while a greater cross-terrain air mass separation was observed over northern California, western Oregon, and Washington.

Archived RUC and RAP 0-h buffer soundings revealed that 81% of northern, and 56% of southern offshore-directed wind-driven wildfires displayed ingredients[17] supportive of mountain-wave and gap winds (see Fig. 10 for a typical mountain-wave sounding). Similarities between northern and southern mountain-wave environments included a critical level situated on average near 600 hPa that was characterized by a combination of flow reversal and a wind speed minimum. Cross-barrier wind direction was also on average east to northeast for both northern and southern events, and the location of peak cross-barrier wind speeds was centered near 900 hPa (Table 4). Differences between the northern and southern analysis areas included 1) cross-barrier wind speeds were stronger for northern events (21 vs 15 m s^{-1}), and 2) the location of the ridgetop stable layer was higher for northern events (794 vs 867 hPa). The mountain-wave and gap wind wildfire regimes were also found to be most prevalent during the coldest and most stable parts of the day. For instance, Fig. 11 shows that northern offshore wind events typically occurred between 1800 and 2359 local time (45%), followed by 0000–0559 and 0600–1159 local time

[17] Those ingredients consist of a ridgetop stable layer, strong cross-barrier flow, and a middle troposphere critical level.

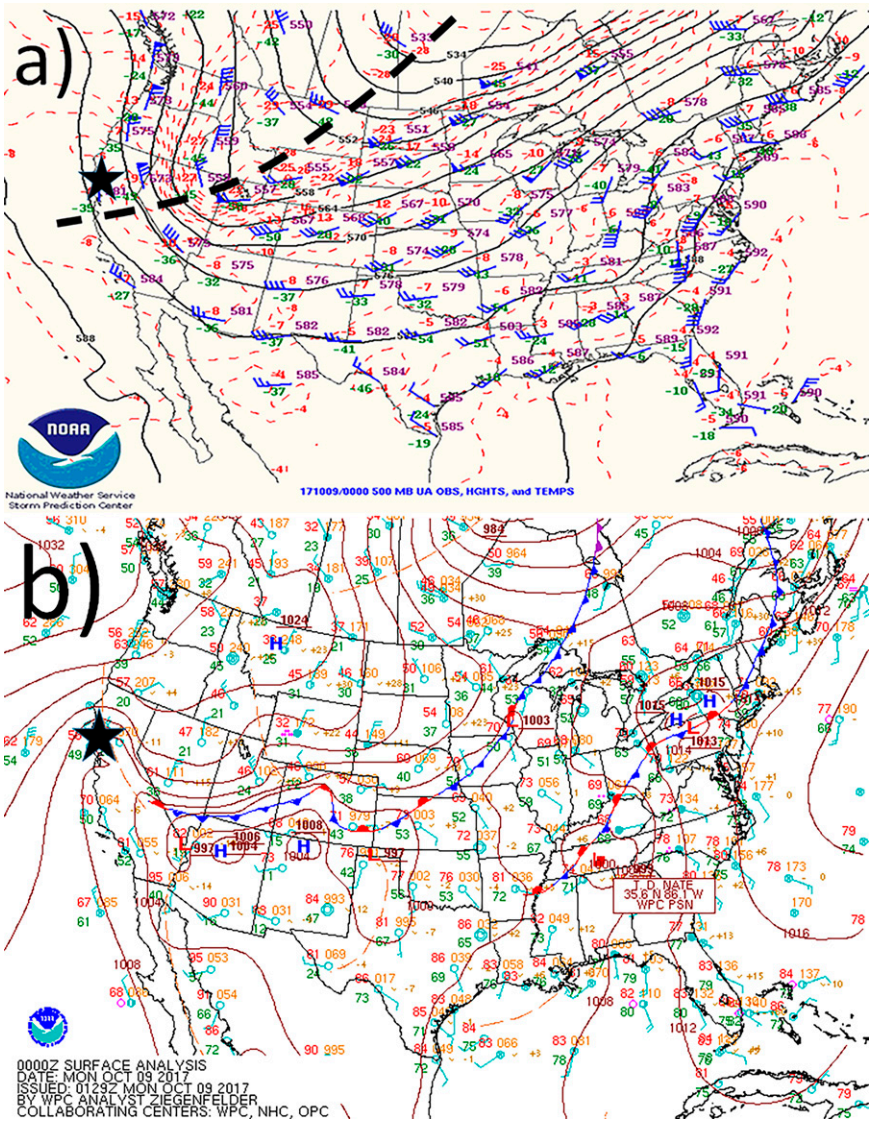

FIG. 6. (a) Upper-air analysis for 500 hPa and (b) surface analysis, both valid at 0000 UTC 9 Oct 2017. The location of a cluster of offshore-directed wind-driven wildfires that initiated shortly after the time of analysis is indicated by the black stars in (a) and (b). Wind barb units in (a) and (b) are knots (1 kt $\approx$ 0.51 m s^{-1}). Temperature (red) and dewpoint temperature (green) units are degrees Celsius in (a) and degrees Fahrenheit in (b). In (a), height (blue) units are decameters (dam) and red temperature contours are in degrees Celsius. Pressure contours (black) in (b) are in hectapascals. The thick broken line in (a) located from southern Canada southwest across California depicts a shortwave trough. A cold front in (b) is depicted from Ontario, Canada, southwest to Kansas and then west to southern Nevada. Areas of surface low pressure and high pressure are annotated in (b) with a red "L" and blue "H," respectively. The maps in (a) and (b) are provided through the courtesy of the NOAA/NWS/NCEP Storm Prediction Center and Weather Prediction Center, respectively.

(20%)—with southern offshore events occupying a similar time range. On the other hand, non-offshore events across the north and south were most likely to occur during the afternoon hours from 1200 to 1759 local time (60% and 57%, respectively). The authors speculate that the offshore-directed wind events were more likely during the evening, night, and morning because that is when 1) cross-barrier flow was strongest as a result of upstream low-level temperatures reaching a minimum, and 2) the ridgetop stable layer was most pronounced when insolation was absent.

Observed winds for the northern and southern offshore-directed fires averaged across valley and ridgetop weather stations displayed small offsets in median values (11 and 13 m s^{-1}, respectively) and large interquartile overlap (Fig. 12). However,

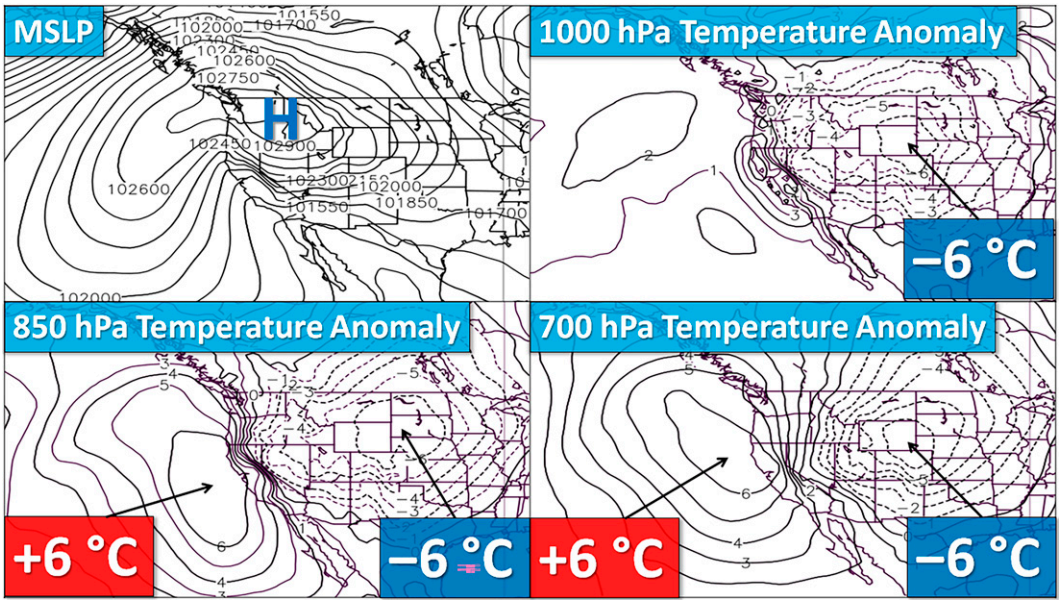

FIG. 7. (top left) Mean sea level pressure (MSLP; Pa), (top right) 1000-hPa temperature anomalies (°C), (bottom left) 850-hPa temperature anomalies (°C), and (bottom right) 700-hPa temperature anomalies (°C) composited using the North American Regional Reanalysis for all northern and southern offshore-directed wind-driven wildfires examined for the period 2000–21. An MSLP high pressure center ("H") located in the vicinity of eastern Washington, eastern Oregon, and western Idaho is annotated in the MSLP composite, and positive (+) and negative (−) temperature anomalies are annotated in the 1000-, 850-, and 700-hPa charts. The maps were provided by the NOAA/ESRL/Physical Sciences Laboratory (https://psl.noaa.gov/cgi-bin/data/narr/plotday.pl).

there is evidence that the most extreme southern offshore-directed events were windier based on a 90th-percentile wind speed value of 25 m s^{-1}, which was 4 m s^{-1} stronger than the northern offshore 90th-percentile value. Those higher speeds may reflect upon the colder environment located upstream from Southern California terrain barriers, which would force stronger cross-barrier winds. Temperature boxplots (Fig. 13) lend credence to that hypothesis. For example, the southern offshore median value was 4°C colder than northern events, and the 25th-percentile value was 2°C colder. It is also evident that non-offshore events occurred in a much warmer air mass than did offshore events, which is likely due to offshore wind events primarily occurring during the autumn and winter, as well as at night, and non-offshore events occurring almost exclusively during the summer, and usually in the afternoon hours. Otherwise, southern offshore events were associated with the driest air masses, as seen by the full interquartile separation in surface RH values displayed in Fig. 14. The combined effects of strong Southern California offshore-directed winds and low RH yielded FFWI values displaying an interquartile range from 59 to 100, which was offset by a full quartile from northern FFWI values that ranged from 45 to 73, and 10th percentile values that were essentially equivalent to the 75th percentile non-offshore FFWI values (Fig. 15). Based on these surface fire parameters alone, Southern California offshore-directed wildfire environments were arguably more extreme than the northern analysis area—yet the impacts in terms of death and destruction were higher over the north.

c. *Fuels and fire ignition*

Annual precipitation near the site of wildfires in this study ranged from around 38 cm at a latitude of 34°N (Southern California), to 51–127 cm over far northern California (latitude of 36°–42°N), to 127–178 cm west of the Oregon and Washington Cascade Range (Fig. 16). This study did not identify extreme wildfire events where precipitation values fell below the threshold typical of Southern California deserts (25 cm), assumingly because vegetation was too sparse to support large fire growth. Instead, Southern California fires occurred where yearly precipitation exceeded 31 cm, which favored fuels such as chaparral that became mixed with grass as yearly precipitation values increased beyond 51 cm. Grass and chaparral fuel biomes occurred northward across northern California and Oregon, but coniferous forested lands also contributed to that fuel landscape. That was followed by a transition to moist temperate coniferous forest across the west side of the Northern Cascade Range in Washington, where yearly precipitation values exceeded 127 cm. That transition is believed to have reduced the potential for extreme wildfires due to greater year-round fuel moisture—though the effects of climate change could cause a gradual shift in vegetation character during the future (Halofsky et al. 2018).

Objective measures of fuel type based on gridded analyses of the 40 Fire Behavior Fuel Models (Scott and Burgan 2005) show that nearly 100% of the wildfires occurring within the Transverse and Peninsular Ranges in Southern California were associated

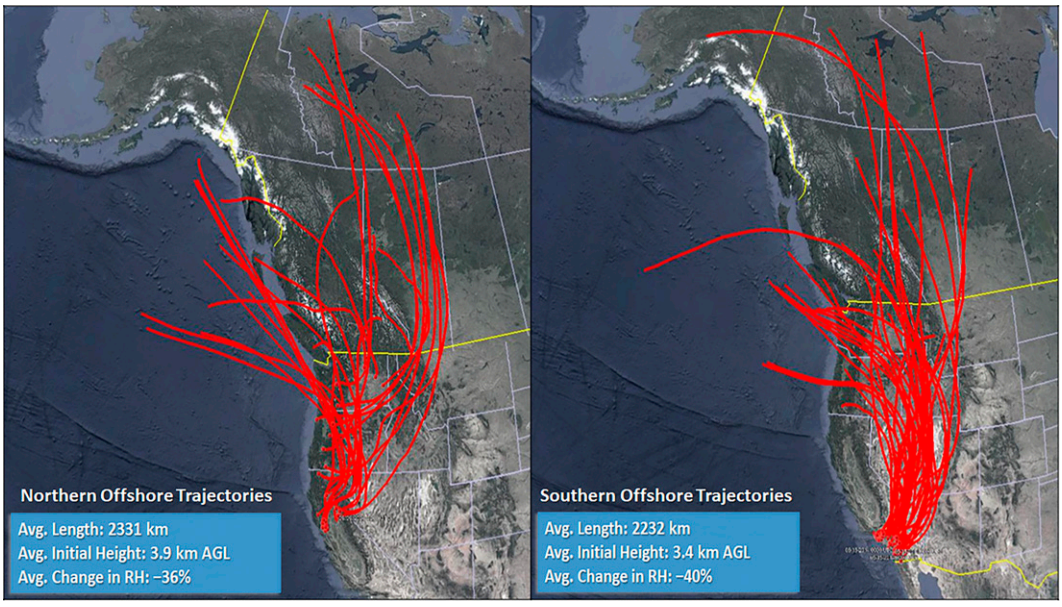

FIG. 8. An analysis of 48-h backward parcel trajectories for (left) northern and (right) southern offshore-directed wind-driven wildfires examined for the period 2000–21. The insets in both plots include the average backward parcel trajectory length (km), the average initial upstream height of parcel trajectories (km AGL), and the average change in RH from the beginning and end points of each parcel trajectory.

with grass and shrub fuel classifications (Fig. 17)—while wildfires occurring north of 37°N latitude (with the exception of the Okanagan Plateau) generally took place in a mixture of fuel types ranging from timber, grass, and shrub. Greater fuel diversity over northern California and western Oregon may have influenced fire intensity and extreme wildfire behavior. For example, crowning and torching associated with timber fuels might yield increased potential for long-distance spot fires due to greater energy release (Storey et al. 2020), which can subsequently dominate the spreading process of the fire front during conflagrations and overwhelm control efforts (Rothermel 1991; Koo et al. 2010).

Analysis of fire start data revealed that offshore-directed wind-driven fires were more likely to be human caused in both the northern (84%) and southern (79%) analysis areas, while non-offshore-directed events in both the north and south had

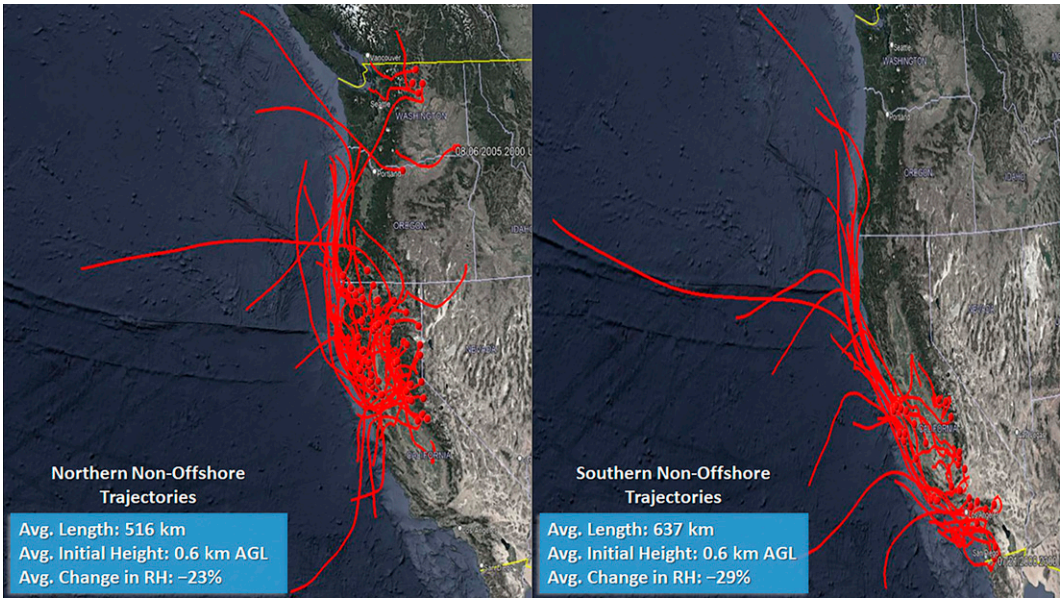

FIG. 9. As in Fig. 8, but for non-offshore-directed wind-driven wildfires.

TABLE 3. Summary of model backward parcel trajectory variables associated with wildfires occurring during the period 2000–21 for offshore-directed winds occurring north of 37.45°N latitude (offshore north) and south of 37.45°N latitude (offshore south) and non-offshore-directed wind-driven wildfires occurring north of 37.45°N latitude (non-offshore north) and south of 37.45°N latitude (non-offshore south). Trajectory length is the mean total horizontal distance traveled (km). The mean initial height of the parcel is given in kilometers AGL, and the mean change in RH represents the difference in RH between the start and end points of the trajectory.

	Trajectory length	Initial parcel height	RH change
Offshore north	2331	3.9	−36%
Offshore south	2232	3.4	−40%
Non-offshore north	516	0.6	−23%
Non-offshore south	637	0.6	−29%

a lower percentage attributed to human activity (58% and 51%, respectively). More specifically, Fig. 18 shows that an electrical source of ignition, such as power line equipment malfunctions, or power line interactions with trees and other vegetation, produced the majority of northern and southern offshore-directed fire starts (54% and 36.8%, respectively). However, a large number of southern offshore-directed events were also ignited by uncontrolled open flames (26.3%). In contrast, lightning was the primary source of ignition for northern non-offshore-directed fires (30.2%), whereas heat and sparks from vehicles were the main source of ignition during southern non-offshore events (17.1%). Electrical ignition sources have proven to be particularly problematic across California and Oregon because they often take place in inaccessible locations that impede initial attack, such as the Camp Fire that destroyed Paradise (St. John et al. 2018), and they can severely deplete initial attack resources when wind-driven electrical ignitions occur simultaneously in clusters across a region, which was observed during the initial stages of the Tubbs Fire of 2017 that destroyed portions of Santa Rosa, California. Other fires, such as the 2003 San Diego County Fire Siege that claimed 16 lives and destroyed 3241 structures (U.S. Forest Service 2022), and the 2020 Beachie Creek Fire in Oregon, also grew out of control across inaccessible locations and then evolved downstream into deadly conflagrations as they became collocated with wind corridors (Syphard and Keeley 2015).

Archived measures of fuel dryness were not analyzed in this study, but an approximation was deduced from the U.S. Drought Monitor. Offshore-directed wind-driven wildfires were associated with an average drought intensity classification of moderate (a value of 1 on a scale from 0 to 4) across the northern and southern study areas. However, excessive drought was not necessary for high-impact offshore-directed wind-driven wildfires. For example, extreme events, such as the 8 November 2018 wildfire that destroyed Paradise as well as the North Bay outbreak on 8 October 2017 that impacted Santa Rosa and the surrounding area, were associated with a drought status of zero. Instead, it is more likely that an entire summer of warm to hot temperatures and near-zero rainfall, which is typical of Oregon and California, yields fire-receptive fuels by the time offshore winds occur during autumn. For instance, climatological records at the site of all northern and southern offshore-directed wind-driven fire locations show a mean maximum temperature during the June–August time period of 29°C, and average summer rainfall ranges from

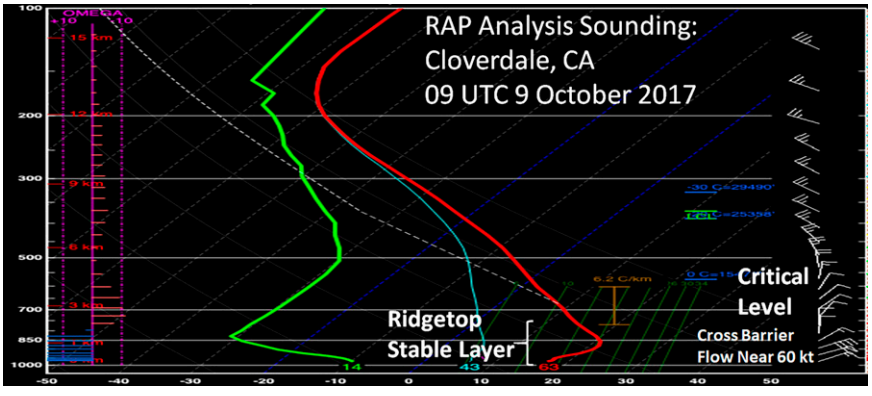

FIG. 10. A skew T diagram from the 0-h RAP model analysis sounding near Cloverdale, California (CVD), valid at 0900 UTC 9 Oct 2017. Pressure (hPa) is plotted on the left, and wind direction and speed (kt) are plotted on the right. The environmental temperature trace is in red (°C), and the environmental dewpoint trace is in green (°C). Annotated features include a ridgetop stable layer, northeasterly cross-barrier winds near 60 kt (31 m s^{-1}), and a critical level where wind speed is near a minimum in magnitude and wind direction reverses from northeast in the low-levels to northwest in the upper-levels of the atmosphere.

TABLE 4. Mean values for mountain-wave ingredients associated with northern and southern offshore-directed wind-driven wildfires derived from RUC and RAP 0-h-analysis proximity soundings valid from 2011 to 2021. Parameters include cross-barrier flow (m s^{-1}), the direction of cross-barrier flow (°), the pressure level of maximum cross-barrier flow (hPa), the central location of the ridgetop stable layer (hPa), the critical level location (hPa), the percentage of critical levels composed of flow reversal, the percentage of critical levels composed of a speed minimum, and the percentage of critical levels composed of both flow reversal and a speed minimum.

	Cross-barrier speed	Cross-barrier direction	Cross-barrier location	Stable layer location	Critical level location	Flow reversal	Speed min	Reversal + min
Offshore north	21	80°	900	794	616	5%	11%	84%
Offshore south	15	59°	929	867	583	5%	10%	85%

1.2 cm across the northern analysis area to 0.25 cm over the southern area. Conversely, low summer precipitation totals are also typical of areas with abundant fuels from western Washington south along the immediate Oregon and northern California coast, but the lack of extreme summer heat, evident by mean maximum temperatures ranging from 15° to 27°C, precludes acute desiccation of vegetation. Yet another factor that might yield critically dry fuels going into the autumn season is the occasional delayed onset of cool-season rainfall. For example, Paradise averages 16.6 cm of precipitation during November but experienced 0.0 cm during November 2018. That allowed fuels to remain cured going into the driest and windiest part of the year, which may have contributed toward extreme outcomes observed during the Camp Fire.

d. *Societal factors*

The WUI is generally designated as the place where human presence, often in the form of housing, meets or overlaps with wildlands such as forests (Stewart et al. 2007). Hammer et al. (2007) showed that in California, housing growth within the WUI during the 1990s was largest across relatively low population regions such as the Sierra Nevada foothills. Those areas were displaced from the larger growth regions of Southern California, where U.S. census data show 100-yr increases ranging from 2500% to 4200%. Those values of growth are 4–8 times as high as the population change for counties impacted by extreme fires in Washington, western Oregon, and northern California. Furthermore, population density was over 10 times as large for Southern California fire-impacted counties as for northern California and western Oregon. Such large population density and growth across Southern California has occurred in the midst of environmental conditions that were often favorable for extreme wildfires. Nevertheless, the deadliest and most destructive wildfires were observed in more sparsely populated northern California and western Oregon. That seemingly paradoxical outcome may partially be explained by data extracted from an extensive WUI analysis recently performed by Radeloff et al. (2017, 2018), which revealed that the percentage of housing and population intermixed with fuels in northern counties impacted by extreme wildfires was ~6 times that of southern counties, and the percentage of housing and population situated adjacent (interfaced) to fuels was ~50% larger (Table 5). This result suggests that, as humans have increased their community presence in the wildlands of northern California and western Oregon—a phenomenon Ashley et al. (2014) term the

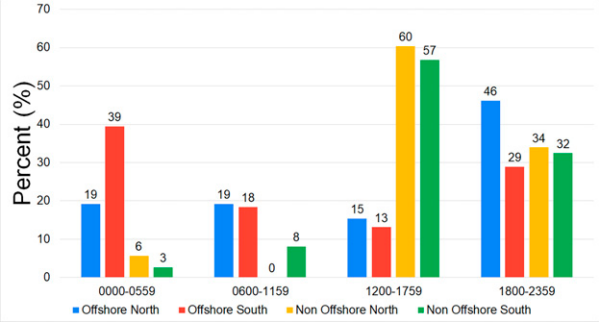

FIG. 11. Percent distribution of extreme wildfire events by local time of day for the period 2000–21 for offshore-directed wind events occurring north of 37.45°N latitude (Offshore North) and south of 37.45°N latitude (Offshore South) and for non-offshore-directed wind-driven wildfires occurring north of 37.45°N latitude (Non Offshore North) and south of 37.45°N latitude (Non Offshore South).

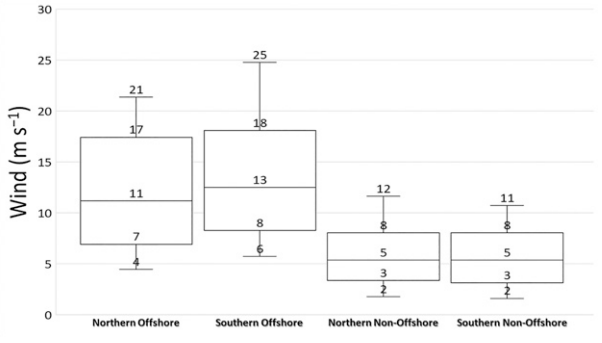

FIG. 12. Box-and-whisker plots of observed wind speed (m s^{-1}) for combined valley and ridgetop wildfire locations measured by ASOS, AWOS, or mesonet observing stations located closest to extreme wildfires analyzed during the period 2000–21. The four boxes represent northern offshore-directed wind-driven wildfires (Northern Offshore), southern offshore-directed wind-driven wildfires (Southern Offshore), northern non-offshore-directed wildfires (Northern Non-Offshore), and southern non-offshore-directed wildfires (Southern Non-Offshore). The boxes span the 25th–75th percentiles, and the whiskers extend up to the 90th and down to the 10th percentiles. The median value is the solid horizontal line located within the boxes.

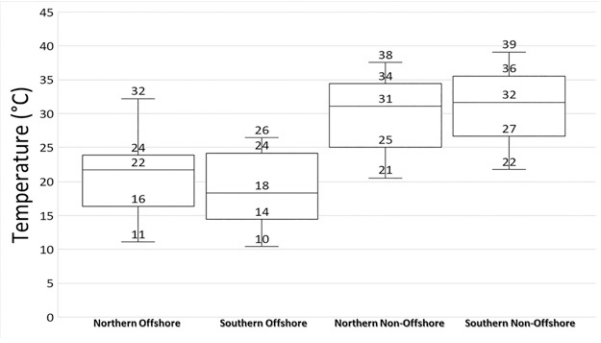

FIG. 13. As in Fig. 12, but for temperature (°C).

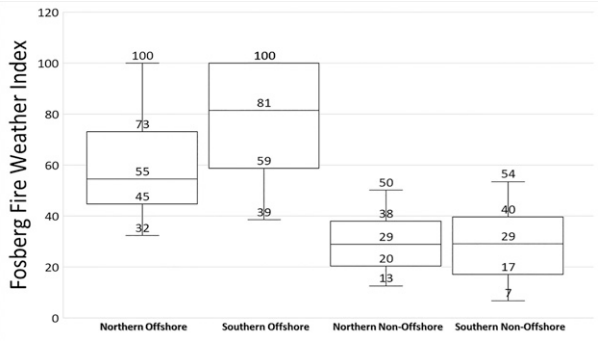

FIG. 15. As in Fig. 12, but for the FFWI. Maximum FFWI values are capped at 100.

"expanding bull's-eye effect," they are experiencing a rise in extreme wildfire exposure that has become a risk realized during events such as the 2018 Camp Fire.

An additional factor contributing to extreme wildfire outcomes was demographical in nature. The median age for counties in the northern analysis area impacted by offshore-directed wind driven wildfires was 41.7 yr, and the average percentage of county population over the age of 65 was 20.9%, which was 5.8 yr and 6.5 percentage points larger, respectively, than counties impacted in Southern California (Table 6). This likely supported fatality outcomes in which the median victim age was nearly 10 years older across northern California and western Oregon, as well as an interquartile fatality range of 65–74 that almost exceeded 75th percentile values for the three other fire regimes analyzed (Fig. 19). Those differences are important for several reasons. For instance, a best approximation of the elapsed time between offshore-directed fire starts and impacts on humans averaged less than a day and was sometimes as low as a few hours, such as the Tubbs Fire of 8–9 October 2017, which began to burn through the city of Santa Rosa around 3 h after initiation, and the 8 November 2018 Camp Fire, which reached the city limits of Paradise ~2 h after the fire started. Elderly persons are at a disadvantage during those scenarios because fast-moving fires require rapid recognition of the threat and the physical ability to quickly evacuate. Those factors consistently reappeared during the deadliest fires across the northern analysis area, with documented fatalities in the elderly population occurring when victims failed to flee because of preexisting injury, confinement to wheelchairs, difficulty operating vehicles, and illness causing some to be bedridden. In addition, there were documented instances in which victims seemingly failed to perceive the immediate wildfire threat because of dementia, social isolation, and technology challenges, whereas others displayed a general apathy toward evacuation (Garner et al. 2020).

In addition to age, fatalities were assessed based on their physical location, with three primary settings identified: a structure (often a home), inside a vehicle, and fleeing outdoors on foot. The northern analysis area was most frequently associated with a fatal structure setting during offshore-directed wind-driven wildfires (61%), while 53% of analyzed fatalities occurring during non-offshore-directed wind-driven Southern California wildfires were associated with victims fleeing on foot. Both northern and southern offshore-directed wind-driven wildfires displayed a similar distribution of victims dying while either inside a vehicle (12% and 18%, respectively) or while fleeing on foot (23% and 25%, respectively). Fatalities occurring while fleeing in a vehicle or on foot often

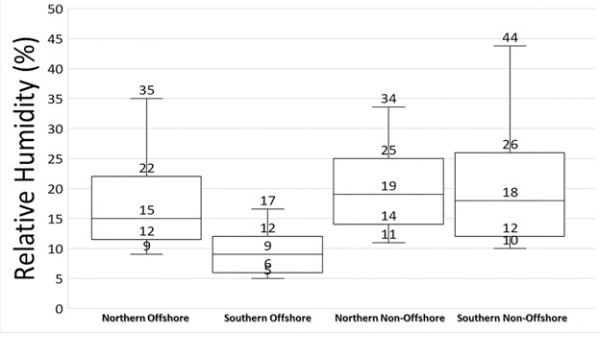

FIG. 14. As in Fig. 12, but for relative humidity (%).

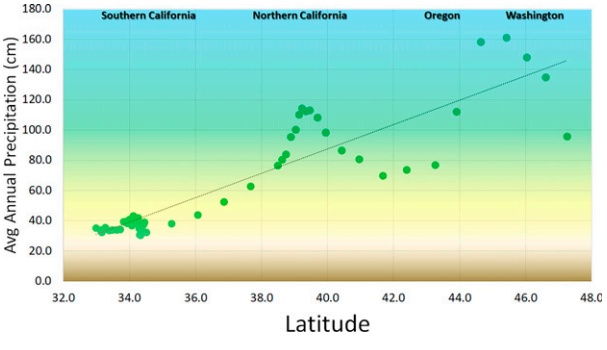

FIG. 16. Average annual precipitation (green dots; cm) and trend line vs latitude for wildfires analyzed during the period 2000–21. State locations are annotated. Desert vegetation occurs with yearly precipitation totals of ≤25 cm, semiarid grasses are associated with precipitation totals between 25 and 51 cm, chaparral generally occurs in the 38–99-cm range, temperate deciduous forests occur from 76 to 127 cm, and moist temperate coniferous forest biomes are associated with yearly precipitation in excess of 127 cm.

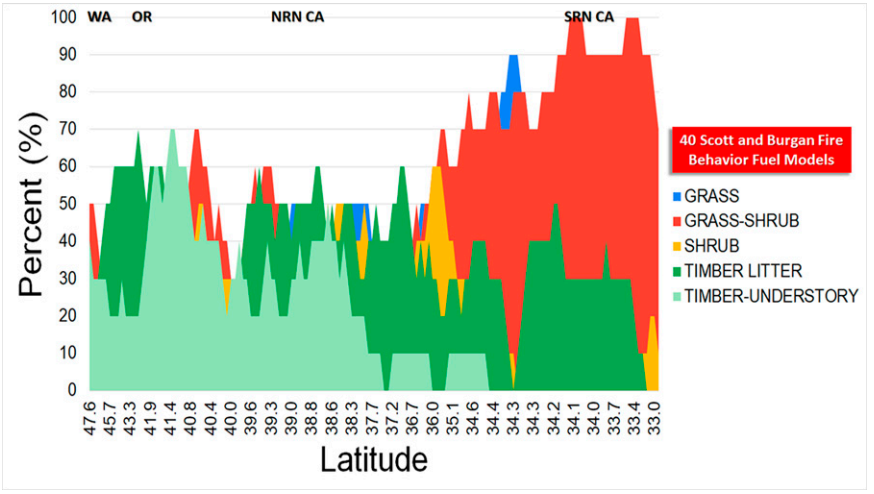

FIG. 17. Fuel type for a 10-point latitudinal moving average from north to south associated with wildfires analyzed from 2000 to 2021. Fuel type was determined at the latitude and longitude for each wildfire by extracting data from gridded information about 40 Scott and Burgan Fire Behavior Fuel Models obtained online (https://landfire.gov/fbfm40.php). Washington (WA), Oregon (OR), northern California (NRN CA), and Southern California (SRN CA) are annotated.

emerged when dangerous gridlock on roadways developed as a result of mass evacuation of communities, with fatalities observed as motorists became entrapped and overtaken by fire burning across roads. For example, there were numerous instances of vehicles catching on fire and melting as traffic jams developed in response to the complete evacuation of Paradise (Maranghides et al. 2021), which led to the entrapment of civilians and emergency responders. Similar citywide evacuations ahead of approaching wildfire have occurred during the 2018 Woolsey Fire in Malibu, California (County of Los Angeles 2019), which led to dramatic images of standstill traffic on the Pacific Coast Highway as an enormous smoke column approached the coast. In addition, the relatively small 15 July 2015 North Fire burned across Interstate 15 in Cajon Pass, resulting in commuters fleeing the scene on foot as tens of vehicles burned along the freeway (Gabbert 2015). Mass evacuation of large communities have also occurred in response to short-term tornado threats (Hatzis and Klockow-McClain 2022). However, in those instances sheltering in place within a sturdy structure is the recommended best action, whereas in wildfires civilians have almost no choice but to flee.

5. Conclusions and discussion

The environments and impacts associated with offshore-directed wind-driven wildfires that posed an immediate threat to life and property across the Pacific Coast states have been examined. Those events occurred with a well-documented surface and upper-air pattern featuring anomalous midlevel ridge amplification over the northeast Pacific

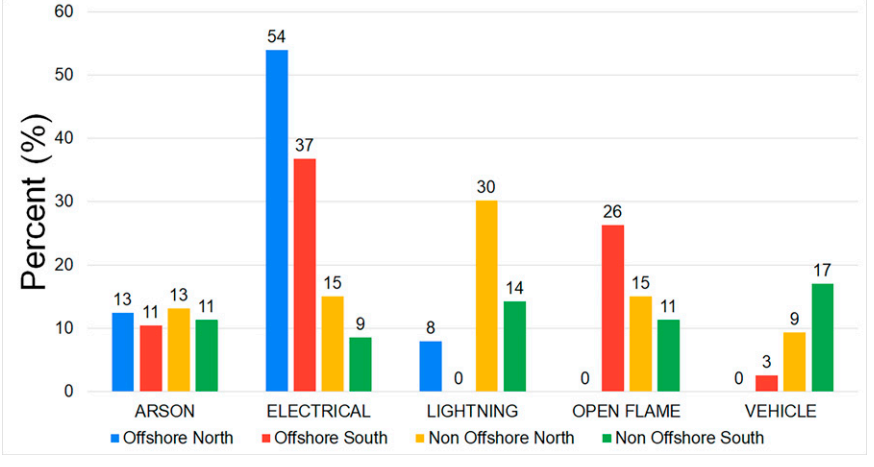

FIG. 18. Similar to Fig. 11, but for the source of wildfire ignition.

TABLE 5. WUI information from Radeloff et al. (2017) for northern offshore-directed events (offshore north), southern offshore-directed events (offshore south), northern non-offshore-directed events (non-offshore north), and southern non-offshore-directed events (non-offshore south). The symbol IM represents intermixed, and IF represents interfaced. The symbols %AREA IM and %AREA IF are the percentage of wildfire county area intermixed or interfaced, respectively, with fuels; %HOUSING IM and %HOUSING IF are the percentage of wildfire county housing stock intermixed or interfaced, respectively, with fuels; and %POP IM and %POP IF are the percentage of wildfire county population intermixed or interfaced, respectively, with fuels.

	%AREA IM	%AREA IF	%HOUSING IM	%HOUSING IF	%POP IM	%POP IF
Offshore north	10.2%	2.7%	23.0%	43.8%	21.7%	44.2%
Offshore south	5.9%	5.5%	3.4%	28.7%	3.0%	27.5%
Non-offshore north	6.6%	1.2%	38.1%	43.3%	35.5%	43.5%
Non-offshore south	6.9%	3.4%	7.5%	32.7%	6.0%	30.6%

Ocean, a surface anticyclone and cold low-level temperature anomaly positioned along the east side of the Sierra Nevada and Cascade Range, and subsequent development of strong offshore-directed cross-barrier flow (National Weather Service 1999; Huang et al. 2009; Mass and Ovens 2019; McClung and Mass 2020; Mass and Ovens 2021; Mass et al. 2021). It was inferred that the cross-barrier winds combined with a ridgetop stable layer and critical level in the middle troposphere favored intense gap winds and mountain-wave development that supported extreme fire behavior and spread—particularly during the evening, night, and morning hours when cross-barrier flow and ridgetop stable layers are strongest due to maximal low-level cooling upstream of north–south-oriented terrain (Doran and Zhong 2000; Sharp and Mass 2004; Hughes and Hall 2010; Abatzoglou et al. 2013; Neiman et al. 2019). Fire ignitions were often human caused (electrical), sometimes occurred in clusters, and when they became collocated with gap and mountain-wave winds, rapidly spread downstream toward populated areas. Factors such as drought were not found to be a necessary ingredient for extreme offshore-directed wind-driven conflagrations across the Pacific Coast states. Instead, prolonged heat that is typical of summer across interior portions of California and Oregon combined with near-zero warm-season rainfall appeared to sufficiently cure fuels that were primed to burn by the time offshore winds became favorable during autumn.

Extreme offshore-directed wind-driven wildfires occurred in several different geographic regions. The first was located across the Transverse and Peninsular Ranges of Southern California, while others occurred immediately north of the San Francisco Bay Area, as well as the western foothills of the Sierra Nevada in northern California, and the western slopes of the Oregon Cascade Range. Surface observations associated with offshore-directed events revealed that wind speeds were slightly stronger and relative humidity values were lower during Southern California events, which resulted in more extreme environments depicted by larger FFWI values. Nevertheless, impacts in terms of lives lost and structures destroyed were more severe across northern California and western Oregon due to a Goldilocks zone of factors:

1) northern California and western Oregon counties impacted by offshore-directed wind-driven wildfires were composed of a greater percentage of homes and population that were intermixed with fire-favorable fuels. On the other hand, housing and population located across Southern California fire-prone counties were more displaced from fuels—possibly due to substantial urban sprawl.
2) northern California and western Oregon wildfires igniting upstream from communities were collocated with wind corridors that caused them to spread downstream through a diverse array of fire-receptive fuels. The diversity in fuels, which included timber, shrubs, and grasses, may have favored more extreme fire behavior such as long-range spotting, torching, crowning, and firebrand showers that inhibited fire suppression efforts.
3) northern California and western Oregon communities were composed of a higher percentage of socially vulnerable people such as the elderly, which increased the chance of fatal outcomes during rapidly evolving wildfires due to limitations in perceiving a fast-approaching wildfire and a reduced likelihood of physically evading a fire.

Total population and population density were not found to be essential factors contributing to extreme wildfire outcomes

TABLE 6. Fire and county specific fatality circumstances associated with wildfires analyzed during the period 2000–21 for northern offshore-directed events (offshore north), southern offshore-directed events (offshore south), northern non-offshore-directed events (non-offshore north), and southern non-offshore-directed events (non-offshore south). Median county age and percentage of county over age 65 are only valid for counties impacted by wildfires examined in this study.

Fire regime	Total wildfire fatalities	Median wildfire fatality age	Median county age	Percentage of county over age 65	Wildfire fatality inside structure	Wildfire fatality inside vehicle	Wildfire fatality while fleeing on foot
Offshore north	162	63.8	41.7	20.8%	61%	12%	25%
Offshore south	46	54.8	35.9	14.4%	31%	18%	23%
Non-offshore north	37	48.6	45.1	23.5%	35%	0%	21%
Non-offshore south	18	51.8	34.5	14.1%	24%	6%	53%

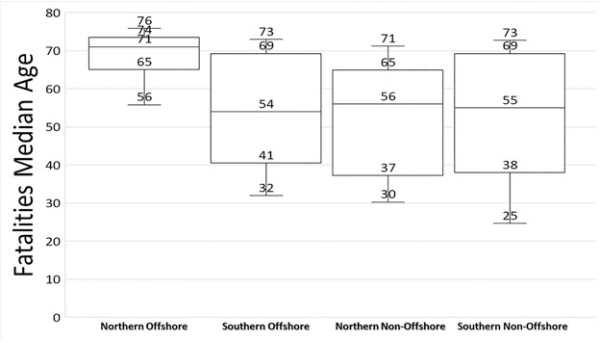

FIG. 19. As in Fig. 12, but for the median age of wildfire fatalities.

across the Pacific Coast states. Instead, impacts were more strongly influenced by the "expanding bull's-eye" of human development within fuels (Ashley et al. 2014). For example, millions of people in the Los Angeles metropolitan area who are exposed to hot, dry, and windy fire-weather conditions during autumn and winter are displaced from dry fire-receptive fuels because of the expansive urban landscape. On the other hand, only a few tens of thousands of people might be exposed to similar weather conditions in northern California and western Oregon, but the vulnerability is significantly higher because communities have developed within the fuels. That is particularly true for communities that are located in close proximity to terrain features that support strong gap and mountain-wave winds, which act to drive fires through population centers. The destruction of property is nearly inevitable when those communities are intermixed with flammable fuels, and many lives may be in jeopardy, particularly when the elderly population is high due to their slower response to fast-evolving wildfires.

The environments, topography, fuel characteristics, and societal factors leading to extreme wildfire outcomes highlighted in this paper dovetail with a relatively new National Weather Service phrase that California offices have the option to include in red flag warnings (RFW) called a "particularly dangerous situation" (PDS). The PDS RFW highlights rare combinations of strong winds, low relative humidity, and dry fuels that could lead to wildfires that are especially impactful to the public and wildland firefighters.[18] Based on the results presented, PDS RFW events across California, Oregon, and Washington are most likely when offshore-directed winds are expected across ridges and terrain gaps, with the most severe combinations of wind and relative humidity often occurring at night. Communities intermixed with fuels and located within terrain favored wind corridors may be most at risk of experiencing adverse impacts, and high fatality outcomes are most probable in communities composed of high numbers of elderly citizens. However, PDS RFW scenarios are not strictly a West Coast phenomenon. The 2021 Marshall Fire is an example of a firestorm occurring in the lee of the Rocky Mountains that became coupled with extreme winds generated by a mountain wave (NOAA Boulder 2022). That fire displayed extreme rates of spread as it swept downstream across the communities of Superior and Louisville, Colorado, resulting in the destruction of 1000 structures and the death of two civilians, both of whom were over the age of 65. It is these types of fires that are coupled with very strong mesoscale and topographically induced winds that operational forecasters, wildland firefighters, government agencies, and news media should be most aware of when anticipating extreme wildfire impacts.

Portions of the elderly population that suffer from cognitive and physical deficits have been identified as experiencing an acute vulnerability to fatal wildfire outcomes—particularly across northern California and western Oregon. Impacts to that age group could potentially be reduced if they had more time to identify and evacuate wildfire threats, or in some cases receive direct outreach and physical assistance during short-term evacuation scenarios. To accomplish that task, advanced planning seems to be especially important in order to balance the safety of those assisting. Weather Ready Nation and the Community Emergency Response Team might be ideally organized to develop readiness and responsiveness that enhances safety within the elderly community during times of severe fire danger. An additional mitigating factor discussed in Garner et al. (2020) could be the involvement of family and neighbors taking the initiative to check in on their elders during times of heightened wildfire risk—which would require preseason public outreach and education on the part of agencies such as the National Weather Service or local, state, and federal fire organizations. Part of the planning process would also include identifying those communities with the greatest risk of experiencing extreme wildfire outcomes. Those communities could be recognized by performing a high-resolution model reanalysis of gap and mountain-wave wind events across the Pacific Coast states, and then overlaying envelopes of certain wind thresholds across population data. That information could be further augmented with geospatial analyses of WUI housing stock as well as demographic information such as population age, all of which could be utilized to inform targeted community planning as well as impact-based messaging when fire-favorable offshore-directed wind events are anticipated.

Acknowledgments. The authors thank Tim Chavez for providing expert guidance on California fuel environments and fire behavior. The reviews, comments, and suggestions provided by James White, Joshua Whisnant, Jeff Tonkin, Alex Dodd, Ryan Aylward, Tyler Jewel, Merl Heinlein, and Troy Nicolini were also greatly appreciated. The authors also express appreciation for the comments and suggestions provided by two anonymous reviewers. The National Weather Service Western Region Headquarters and the Science and Technology Infusion Division are also thanked for supporting this work.

Data availability statement. Many of the data presented in this study are tabulated in a master Excel sheet, which the authors compiled incrementally over time and which is available upon request to the corresponding author. Otherwise, all data

[18] California Fire Weather Annual Operating Plan 2022.

sources and software are freely available online and have been documented throughout the paper. In addition, Fig. 10 was generated using the sounding program SHARPpy (Blumberg et al. 2017).

REFERENCES

Abatzoglou, J. T., R. Barbero, and N. J. Nauslar, 2013: Diagnosing Santa Ana winds in Southern California with synoptic-scale analysis. *Wea. Forecasting*, **28**, 704–710, https://doi.org/10.1175/WAF-D-13-00002.1.

Ashley, W. S., S. Strader, T. Rosencrants, and A. J. Krmenec, 2014: Spatiotemporal changes in tornado hazard exposure: The case of the expanding bull's-eye effect in Chicago, Illinois. *Wea. Climate Soc.*, **6**, 175–193, https://doi.org/10.1175/WCAS-D-13-00047.1.

Bahrani, B., 2020: Characterization of firebrands generated from selected vegetative fuels in wildland fires. Ph.D. dissertation, University of North Carolina at Charlotte, 127 pp.

Benjamin, S. G., and Coauthors, 2004: An hourly assimilation-forecast cycle: The RUC. *Mon. Wea. Rev.*, **132**, 495–518, https://doi.org/10.1175/1520-0493(2004)132<0495:AHACTR>2.0.CO;2.

——, and Coauthors, 2016: A North American hourly assimilation and model forecast cycle: The Rapid Refresh. *Mon. Wea. Rev.*, **144**, 1669–1694, https://doi.org/10.1175/MWR-D-15-0242.1.

Blier, W., 1998: The sundowner winds of Santa Barbara, California. *Wea. Forecasting*, **13**, 702–716, https://doi.org/10.1175/1520-0434(1998)013<0702:TSWOSB>2.0.CO;2.

Blumberg, W. G., K. T. Halbert, T. A. Supinie, P. T. Marsh, R. L. Thompson, and J. A. Hart, 2017: SHARPpy: An open source sounding analysis toolkit for the atmospheric sciences. *Bull. Amer. Meteor. Soc.*, **98**, 1625–1636, https://doi.org/10.1175/BAMS-D-15-00309.1.

Brinkmann, W. A. R., 1974: Strong downslope winds at Boulder, Colorado. *Mon. Wea. Rev.*, **102**, 592–602, https://doi.org/10.1175/1520-0493(1974)102<0592:SDWABC>2.0.CO;2.

Chen, W.-D., and R. B. Smith, 1987: Blocking and deflection of airflow by the Alps. *Mon. Wea. Rev.*, **115**, 2578–2597, https://doi.org/10.1175/1520-0493(1987)115<2578:BADOAB>2.0.CO;2.

Clark, T. L., and W. R. Peltier, 1984: Critical level reflection and the resonant growth of nonlinear mountain waves. *J. Atmos. Sci.*, **41**, 3122–3134, https://doi.org/10.1175/1520-0469(1984)041<3122:CLRATR>2.0.CO;2.

Colle, B. A., and C. F. Mass, 1998: Windstorms along the western side of the Washington Cascade Mountains. Part II: Characteristics of past events and three-dimensional idealized simulations. *Mon. Wea. Rev.*, **126**, 53–71, https://doi.org/10.1175/1520-0493(1998)126<0053:WATWSO>2.0.CO;2.

Colman, B. R., and C. F. Dierking, 1992: The Taku wind of southeast Alaska: Its identification and prediction. *Wea. Forecasting*, **7**, 49–64, https://doi.org/10.1175/1520-0434(1992)007<0049:TTWOSA>2.0.CO;2.

County of Los Angeles, 2019: After action review of the Woolsey fire incident. Citygate Associates Rep., 203 pp., http://file.lacounty.gov/SDSInter/bos/supdocs/144968.pdf.

Doran, J. C., and S. Zhong, 2000: Thermally driven gap winds into the Mexico City basin. *J. Appl. Meteor.*, **39**, 1330–1340, https://doi.org/10.1175/1520-0450(2000)039<1330:TDGWIT>2.0.CO;2.

Durran, D. R., and J. B. Klemp, 1987: Another look at downslope winds. Part II: Nonlinear amplification beneath wave-overturning layers. *J. Atmos. Sci.*, **44**, 3402–3412, https://doi.org/10.1175/1520-0469(1987)044<3402:ALADWP>2.0.CO;2.

FEMA, 1995: The East Bay Hills Fire: Oakland-Berkely, California. U.S. Fire Administration Tech. Rep. USFA-TR-060, 130 pp., https://www.caloes.ca.gov/wp-content/uploads/Fire-Rescue/Documents/US-Fire-Admin-East-Bay-Hills-Fire-Report.pdf.

Fosberg, M. A., 1978: Weather in wildland fire management: The fire weather index. *Proc. Conf. on Sierra Nevada Meteorology*, Lake Tahoe, CA, Amer. Meteor. Soc., 1–4.

Gabbert, B., 2015: Carmegeddon: North Fire burns across California interstate, traps cars. *Wildfire Today*, 17 July, https://wildfiretoday.com/2015/07/17/north-fire-burns-across-interstate-traps-cars/.

Garner, J. M., W. C. Iwasko, T. D. Jewel, B. R. Charboneau, A. A. Dodd, and K. M. Zontos, 2020: A multihazard assessment of age-related weather vulnerabilities. *Wea. Climate Soc.*, **12**, 367–386, https://doi.org/10.1175/WCAS-D-19-0124.1.

Goss, M., D. L. Swain, J. T. Abatzoglou, A. Sarhadi, C. A. Kolden, A. P. Williams, and N. S. Diffenbaugh, 2020: Climate change is increasing the likelihood of extreme autumn wildfire conditions across California. *Environ. Res. Lett.*, **15**, 094016, https://doi.org/10.1088/1748-9326/ab83a7.

Halofsky, J. S., D. R. Conklin, D. C. Donato, J. E. Halofsky, and J. B. Kim, 2018: Climate change, wildfire, and vegetation shifts in a high-inertia forest landscape. *PLOS ONE*, **13**, e0209490, https://doi.org/10.1371/journal.pone.0209490.

Hammer, R. B., V. C. Radeloff, J. S. Fried, and S. I. Stewart, 2007: Wildland-urban interface housing growth during the 1990s in California, Oregon, and Washington. *Int. J. Wildland Fire*, **16**, 255–265, https://doi.org/10.1071/WF05077.

Hatzis, J. J., and K. E. Klockow-McClain, 2022: A spatiotemporal perspective on the 31 May 2013 tornado evacuation in the Oklahoma City metropolitan area. *Wea. Climate Soc.*, **14**, 721–735, https://doi.org/10.1175/WCAS-D-21-0106.1.

Huang, C., Y.-L. Lin, M. L. Kaplan, and J. J. Charney, 2009: Synoptic-scale and mesoscale environments conducive to forest fires during the October 2003 extreme fire event in Southern California. *J. Appl. Meteor. Climatol.*, **48**, 553–579, https://doi.org/10.1175/2008JAMC1818.1.

Hughes, M., and A. Hall, 2010: Local and synoptic mechanisms causing Southern California's Santa Ana winds. *Climate Dyn.*, **34**, 847–857, https://doi.org/10.1007/s00382-009-0650-4.

Keeley, J. E., and A. D. Syphard, 2019: Twenty-first century California, USA, wildfires: Fuel-dominated vs. wind-dominated fires. *Fire Ecol.*, **15**, 24, https://doi.org/10.1186/s42408-019-0041-0.

Klemp, J. B., and D. K. Lilly, 1975: The dynamics of wave-induced downslope winds. *J. Atmos. Sci.*, **32**, 320–339, https://doi.org/10.1175/1520-0469(1975)032<0320:TDOWID>2.0.CO;2.

——, and ——, 1978: Numerical simulation of hydrostatic mountain waves. *J. Atmos. Sci.*, **35**, 78–107, https://doi.org/10.1175/1520-0469(1978)035<0078:NSOHMW>2.0.CO;2.

Koo, E., P. J. Pagni, D. R. Weise, and J. P. Woycheese, 2010: Firebrands and spotting ignition in large-scale fires. *Int. J. Wildland Fire*, **19**, 818–843, https://doi.org/10.1071/WF07119.

Lagouvardos, K., V. Kotroni, T. M. Giannaros, and S. Dafis, 2019: Meteorological conditions conducive to the rapid spread of the deadly wildfire in eastern Attica, Greece. *Bull. Amer. Meteor. Soc.*, **100**, 2137–2145, https://doi.org/10.1175/BAMS-D-18-0231.1.

Lareau, N. P., N. J. Nauslar, and J. T. Abatzoglou, 2018: The Carr fire vortex: A case of pyrotornadogenesis? *Geophys. Res. Lett.*, **45**, 13 107–13 115, https://doi.org/10.1029/2018GL080667.

——, ——, E. Bentley, M. Roberts, S. Emmerson, B. Bring, M. Mehle, and J. Wallman, 2022: Fire-generated tornadic vortices. *Bull. Amer. Meteor. Soc.*, **103**, E1296–E1320, https://doi.org/10.1175/BAMS-D-21-0199.1.

Lawson, J., and J. Horel, 2015: Analysis of the 1 December 2011 Wasatch downslope windstorm. *Wea. Forecasting*, **30**, 115–135, https://doi.org/10.1175/WAF-D-13-00120.1.

Manzello, S. L., S. Suzuki, M. J. Gollner, and A. Carlos Fernandez-Pello, 2020: Role of firebrand combustion in large outdoor fire spread. *Prog. Energy Combust. Sci.*, **76**, 100801, https://doi.org/10.1016/j.pecs.2019.100801.

Maranghides, A., and Coauthors, 2021: A case study of the Camp Fire—Fire progression timeline. NIST Tech. Note 2135, 412 pp., https://doi.org/10.6028/NIST.TN.2135.

Martin, J., and T. Hillen, 2016: The spotting distribution of wildfires. *Appl. Sci.*, **6**, 177, https://doi.org/10.3390/app6060177.

Mass, C. F., and M. D. Albright, 1985: A severe windstorm in the lee of the Cascade Mountains of Washington State. *Mon. Wea. Rev.*, **113**, 1261–1281, https://doi.org/10.1175/1520-0493(1985)113<1261:ASWITL>2.0.CO;2.

——, and D. Ovens, 2019: The northern California wildfires of 8–9 October 2017: The role of a major downslope windstorm event. *Bull. Amer. Meteor. Soc.*, **100**, 235–256, https://doi.org/10.1175/BAMS-D-18-0037.1.

——, and ——, 2021: The synoptic and mesoscale evolution accompanying the 2018 Camp Fire of northern California. *Bull. Amer. Meteor. Soc.*, **102**, E168–E192, https://doi.org/10.1175/BAMS-D-20-0124.1.

——, ——, R. Conrick, and J. Saltenberger, 2021: The September 2020 wildfires over the Pacific Northwest. *Wea. Forecasting*, **36**, 1843–1865, https://doi.org/10.1175/WAF-D-21-0028.1.

McClung, B., and C. F. Mass, 2020: The strong, dry winds of central and northern California: Climatology and synoptic evolution. *Wea. Forecasting*, **35**, 2163–2178, https://doi.org/10.1175/WAF-D-19-0221.1.

Mesinger, F., and Coauthors, 2006: North American Regional Reanalysis. *Bull. Amer. Meteor. Soc.*, **87**, 343–360, https://doi.org/10.1175/BAMS-87-3-343.

National Weather Service, 1999: Critical fire weather patterns of the United States. National Interagency Fire Center Rep., 66 pp., https://gacc.nifc.gov/nwcc/content/products/fwx/publications/CRITICAL_FWX_PATTERNS_US.pdf.

Nauslar, N., J. Abatzoglou, and P. Marsh, 2018: The 2017 North Bay and Southern California fires: A case study. *Fire*, **1**, 18, https://doi.org/10.3390/fire1010018.

Neiman, P. J., D. J. Gottas, and A. B. White, 2019: A two-cool-season wind profiler-based analysis of westward-directed gap flow through the Columbia River Gorge. *Mon. Wea. Rev.*, **147**, 4653–4680, https://doi.org/10.1175/MWR-D-19-0026.1.

NOAA Boulder, 2022: The Marshall Fire. Accessed 29 January 2022, https://storymaps.arcgis.com/stories/cd7e211f5d594f9996b061d05670e779.

Radeloff, V. C., and Coauthors, 2017: The 1990–2010 wildland-urban interface of the conterminous United States—Geospatial data: 2nd edition. Forest Service Research Data Archive, accessed 13 January 2022, https://doi.org/10.2737/RDS-2015-0012-2.

——, and Coauthors, 2018: Rapid growth of the US wildland-urban interface raises wildfire risk. *Proc. Natl. Acad. Sci. USA*, **115**, 3314–3319, https://doi.org/10.1073/pnas.1718850115.

Rothermel, R. C., 1991: Predicting behavior and size of crown fires in the northern Rocky Mountains. USDA Forest Service Rocky Mountain Research Station Research Paper INT-438, 46 pp., https://doi.org/10.2737/INT-RP-438.

Scott, J. H., and R. E. Burgan, 2005: Standard fire behavior fuel models: A comprehensive set for use with Rothermel's surface fire spread model. USDA Forest Service General Tech. Rep. RMRS-GTR-153, 72 pp., https://doi.org/10.2737/RMRS-GTR-153.

Sharp, J., and C. F. Mass, 2004: Columbia Gorge gap winds: Their climatological influence and synoptic evolution. *Wea. Forecasting*, **19**, 970–992, https://doi.org/10.1175/826.1.

Stewart, S. I., V. C. Radeloff, R. B. Hammer, and T. J. Hawbaker, 2007: Defining the wildland–urban interface. *J. For.*, **105**, 201–207, https://doi.org/10.1093/jof/105.4.201.

St. John, P., A. M. Phillips, J. Serna, S. Kohli, and L. Newberry, 2018: California fire: What started as a tiny brush fire became the state's deadliest wildfire. Here's how. *Los Angeles Times*, 18 November, https://www.latimes.com/local/california/la-me-camp-fire-tictoc-20181118-story.html.

Storey, M. A., O. F. Price, J. J. Sharples, and R. A. Bradstock, 2020: Drivers of long-distance spotting during wildfires in south-eastern Australia. *Int. J. Wildland Fire*, **29**, 459–472, https://doi.org/10.1071/WF19124.

Syphard, A. D., and J. E. Keeley, 2015: Location, timing and extent of wildfire vary by cause of ignition. *Int. J. Wildland Fire*, **24**, 37–47, https://doi.org/10.1071/WF14024.

Taylor, S. V., D. R. Cayan, N. E. Graham, and K. P. Georgakakos, 2008: Northerly surface winds over the eastern North Pacific Ocean in spring and summer. *J. Geophys. Res.*, **113**, D02110, https://doi.org/10.1029/2006JD008053.

Tohidi, A., and N. B. Kaye, 2017: Stochastic modeling of firebrand shower scenarios. *Fire Saf. J.*, **91**, 91–102, https://doi.org/10.1016/j.firesaf.2017.04.039.

U.S. Forest Service, 2022: The 2003 San Diego County fire siege fire safety review. USDA Rep., 58 pp., https://www.fs.usda.gov/Internet/FSE_DOCUMENTS/stelprdb5297020.pdf.

Westerling, A. L., 2016: Increasing western US forest wildfire activity: Sensitivity to changes in the timing of spring. *Philos. Trans. Roy. Soc.*, **B371**, 20150178, https://doi.org/10.1098/rstb.2015.0178.